



DEGREE PROJECT IN TECHNOLOGY,
FIRST CYCLE, 15 CREDITS
STOCKHOLM, SWEDEN 2020

Modeling Radiation Induced Degradation of Lattice Thermal Conductivity

ROBIN ANDERSSON

Abstract

Nuclear power technology is currently experiencing a revolutionary development process and its utilization is researched and debated throughout the world whereas sustainability is one of the most important topics in the material science arena. Some components in a nuclear power plant are subject to an irradiating environment which will cause significant damage to the material over time. Thus, it is of utmost importance that the affected materials are well-designed for enduring such conditions because of the extensive lifetime of a nuclear power plant. The highly energetic particles that are inherent with nuclear reactions will generate point defects in the microstructure of the material which will alter its macroscopic behavior.

Managing heat is crucial in a nuclear power plant and therefore this thesis is devoted to modeling the degradation effect on the lattice thermal conductivity as a result of the point defects, and to establish the intervening relation. This is achieved by *ab initio* simulations on supercells where the quantum-mechanical forces are calculated with density functional theory and with the generalized gradient approximation for the exchange-correlation term. The phonon Boltzmann equation is solved by linearization and by using the relaxation-time approximation which allows the lattice thermal conductivity to be calculated for the model. The phonon band modes and the phonon density of states is examined as well.

To date there are no reports currently found in the literature where this topic is approached with similar methods.

Sammanfattning

Kärnkraftsteknologin genomgår just nu en revolutionerande utvecklingsprocess och dess användning debatteras över hela världen där hållbarhet är en av de viktigaste ståndpunkterna i materialvetenskapsområdet. Vissa komponenter i ett kärnkraftverk blir utsatta för en bestrålade miljö vilket orsakar stor skada på materialet över tid. Det är därför av högsta vikt att dessa material är designade för att motstå sådana miljöer på grund av kärnkraftverkens långa livstid. De högenergetiska partiklarna som är förekommande vid kärnreaktioner genererar punktdefekter i materialets mikrostruktur vilka ändrar de makroskopiska egenskaperna hos materialet.

Värmehantering är kritiskt i ett kärnkraftverk och därför är detta arbete dedikerat till att modellera effekten av försämring av värmeledningsförmågan i kristallgittret, som resultat av punktdefekterna, och att definiera sambandet. Detta uträttas genom *ab initio* simuleringar av superceller där de kvantmekaniska krafterna beräknas med täthetsfunktionalsteori med en generaliserad approximation av täthetsgradienten för den tillhörande utbytes- och korrelationstermen. Boltzmann ekvationen löses med hjälp av linjärisering och med en approximation av relaxationstiden vilket används för att beräkna värmeledningen i gittret för modellen. Fononernas band-moder och tillståndstäthet undersöks därtill.

För närvarande finns det inga rapporter bland litteraturen där detta ämne behandlas med samma metoder.

Contents

1	Introduction	1
1.1	Theoretical background	2
1.1.1	Radiation damage and point defects	2
1.1.2	Thermal transport and Phonons	9
1.1.3	Boltzmann Transport Equation	12
1.1.4	Density Functional Theory	15
1.1.5	Vienna Ab-Initio Simulation Package	19
1.1.6	Phono3py	20
1.1.7	Phonopy	21
2	Methods	22
2.1	Convergence tests	22
2.1.1	Lattice parameter	23
2.1.2	Energy cut-off parameter	23
2.1.3	Vacancy formation energy	23
2.1.4	Lattice thermal conductivity	24
2.2	Effects of a vacancy	25
2.2.1	Lattice thermal conductivity	25
2.2.2	Phonon band structure and density of states	26
3	Results	27
3.1	Convergence tests	27
3.1.1	Lattice parameter	28
3.1.2	Energy cut-off parameter	29
3.1.3	Vacancy formation energy	30
3.1.4	Lattice thermal conductivity	31
3.2	Effects of a vacancy	33
3.2.1	Lattice thermal conductivity	34
3.2.2	Phonon band structure and density of states	35

CONTENTS

4	Discussion	36
4.1	Social and ethical aspects	37
5	Conclusions and Future Work	39
5.1	Conclusions	39
5.2	Future work	40
6	Acknowledgement	41
7	References	42

Chapter 1

Introduction

A nuclear energy power plant is a safe and efficient facility for production of electricity. With its high and stable delivery capacity, and absence of greenhouse gas emissions, it is a top contender for solving our climate challenges.

In nuclear energy facilities, it is natural that some structural components will be in contact with high levels of radiation, e.g. in segments of the reactor core, or in the spent fuel storage containers. This will cause radiation damage to the metal components which will affect the mechanical properties of the metal in several ways. The radiation contains large amounts of energy which gets absorbed by some of the atoms, causing them to get displaced from their equilibrium state. This is resulting in vacancy and self-interstitial build-up in the lattice structure, which will, amongst other things, dampen the transport properties in the lattice, both on the electronic subsystem and for the phonons.

For pure, perfect metals, and for temperatures near absolute zero, electronic conduction is the main factor for thermal transport, but as soon as the temperature rises or a material microstructure develops due to irradiation, the phonons will take over as the main heat-conducting mechanism. Consecutively, the thermal conduction ability will be reduced as a function of absorbed dose of radiation. This event is very important because managing heat fluxes and local temperatures is crucial in a nuclear energy power plant.

The aim of the work is to establish a relation between the phonon contribution to the lattice thermal conductivity (LTC) and the effects of a vacancy, representing the most basic effect of irradiation. This is investigated by performing *ab initio* simulations on large supercells where the Schrödinger equation

is solved with the Vienna Ab-Initio Simulation Package (VASP) that applies density functional theory (DFT). The phonon Boltzmann transport equation (BTE) is solved by linearization and with the relaxation-time approximation in the phono3py software. Comparisons will be made between models of a 16 atom supercell, and a 15 atom supercell with a vacancy in the central position. The simulated models reveal the phonon interactions throughout the whole supercell by calculating both the frequencies and the group velocities of the phonons. The LTC is calculated in a temperature range from 0 to 1000 K. These properties will be investigated relative to each other in order to determine the effects of a vacancy.

To date there are no reports currently found in the literature where the vacancy effects on the LTC are approached by simulation of atomic-scale models.

As a conclusion, the knowledge of this phenomenon on the atomic scale is fundamental for further utilization on micro and macro scale applications. So, this report will act as a stepping-stone for a more sustainable design of materials in radiation zones, and ultimately, more durable and safer nuclear reactors.

1.1 Theoretical background

The information that is presented in this section is meant to give the reader a fundamental background of the various topics treated in the report, and to act as a support for apprehending the results and conclusions. The details are broadened to provide a fuller understanding of each topic as a whole, and not only for the narrow scope of the report.

1.1.1 Radiation damage and point defects

Radiation of different types are present in the nuclear reactor core, namely alpha-, beta-, gamma-, and neutron radiation. The range of the alpha- and beta radiation is short and rarely reaches out of the fuel rods, which makes it being of no concern considering the radiation damage aspect of the surrounding metal components. The range of gamma- and neutron radiation is longer, which makes them both capable of causing damage to the structures surrounding the reactor core. The majority of the radiation damage is caused by neutrons since the momentum of the neutrons is generally orders of magnitude higher than of the photons in gamma radiation.

Radiation damage event

Neutrons are relatively heavy in mass and can cause structural changes in the bulk of the material which is referred to as radiation damage. The event of radiation damage and its consequences in metals will be briefly worked through in this section with a focus on point defects since it is of high interest. The definition of the radiation damage process is the transfer of the energy from an incident particle to its collision point in the solid and the resulting damage debris in the otherwise perfect crystal lattice, as an effect from the collision. In order to describe the event in detail, it is preferably divided into a number of distinct processes. The first being the incident particle colliding with an atom in the crystal lattice, causing a transfer of kinetic energy from the particle to the lattice atom and by that, generating a primary knock-on atom (PKA). This collision is considered to be quasielastic because some energy is lost to the surrounding electrons, but that amount is negligible due to the weak neutron-electron scattering cross-section. Further, the PKA gets displaced from its original lattice site and travels through the lattice creating additional knock-on atoms in the process. Until the PKA has come to rest as an interstitial atom, the concluding result of this event is a cluster of point defects consisting of empty lattice sites (vacancies) and atoms that settles in between lattice sites (interstitials), which in combination is known as a Frenkel-pair (FP). For radiation-induced interstitials in metals it is documented that instead of taking the regular interstitial position (octahedral for BCC and tetrahedral for FCC), the atom shares the lattice orientation of an already present atom [1]. This leaves the atoms in a metastable state formed as a dumbbell at the resident lattice position. It is classified as a point defect called a self-interstitial atom (SIA), which can be reviewed in figure 1.1.

Threshold displacement energy and displacements per atom

In order for the incident particle to create a FP, its kinetic energy needs to surpass a certain level defined as the threshold displacement energy (TDE), which is the minimum needed kinetic energy transferred by the incident particle to the PKA to create a stable FP. The TDE varies for different materials and is widely studied starting from Milton Burton's report in 1946 [2] continuing with applications by Frederick Seitz in 1949 [3]. Typical values of the TDE ranges from 20 to 100 eV for various materials. For example, the average value referenced by ASTM for the TDE in iron is 40 eV [4]. If the PKA receives less energy than the TDE, it will stay in its lattice site and the absorbed energy will transmit as heat in the material. Since the kinetic energy of a fast neutron sur-

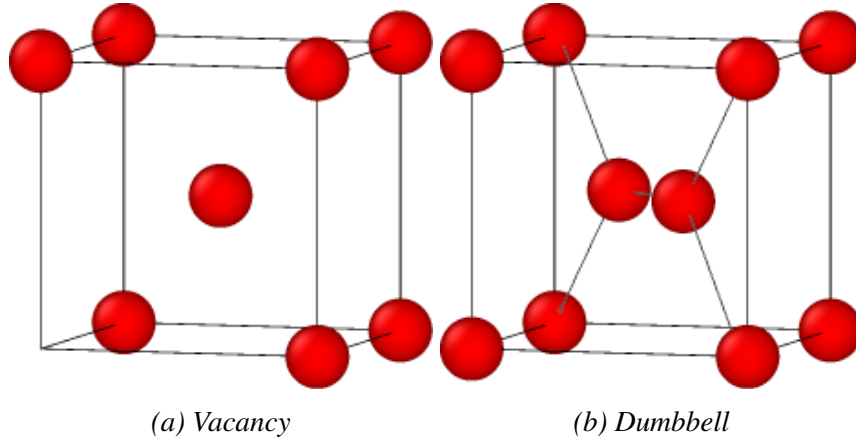


Figure 1.1: The components of a Frenkel-Pair in BCC generated by radiation damage where (a) shows a vacancy and (b) a self-interstitial atom. An additional atom in the centre lattice position, retaining a metastable state.

passes 1 keV, in fact, it is often in levels of MeV, thus containing sufficient kinetic energy to surpass the TDE by a few orders of magnitude. This is the explanation of the cluster of point defects that are produced in the radiation damage event and is shown in figure 1.2.

It is of certain interest to measure the amount of point defects created in the radiation damage event, whereby the Kinchin-Pease model [6] has been developed. The Kinchin-Pease (KP) model is a simplification of the number of point defects created in the event by assuming that all collisions are fully elastic, the number of point defects generated is proportional to the energy transfer of the incident particle to the PKA, and that no point defects annihilates during the process. Equation 1.1 is describing the number of point defects generated by the PKA based on its kinetic energy, T , and the number of point defects generated, $v_{KP}(T)$, is given by:

$$v_{KP}(T) = \begin{cases} 0 & , T < T_{tde} \\ 1 & , T_{tde} < T < 2T_{tde} \\ \frac{T}{2T_{tde}} & , 2T_{tde} < T < T_{lim} \\ \frac{T_{lim}}{2T_{tde}} & , T \geq T_{lim} \end{cases} \quad (1.1)$$

with the threshold displacement energy, T_{tde} , and T_{lim} being an upper limit for the number of displacements which is an assumption made in the KP model which states that that the number of generated point defects is constant above a certain temperature.

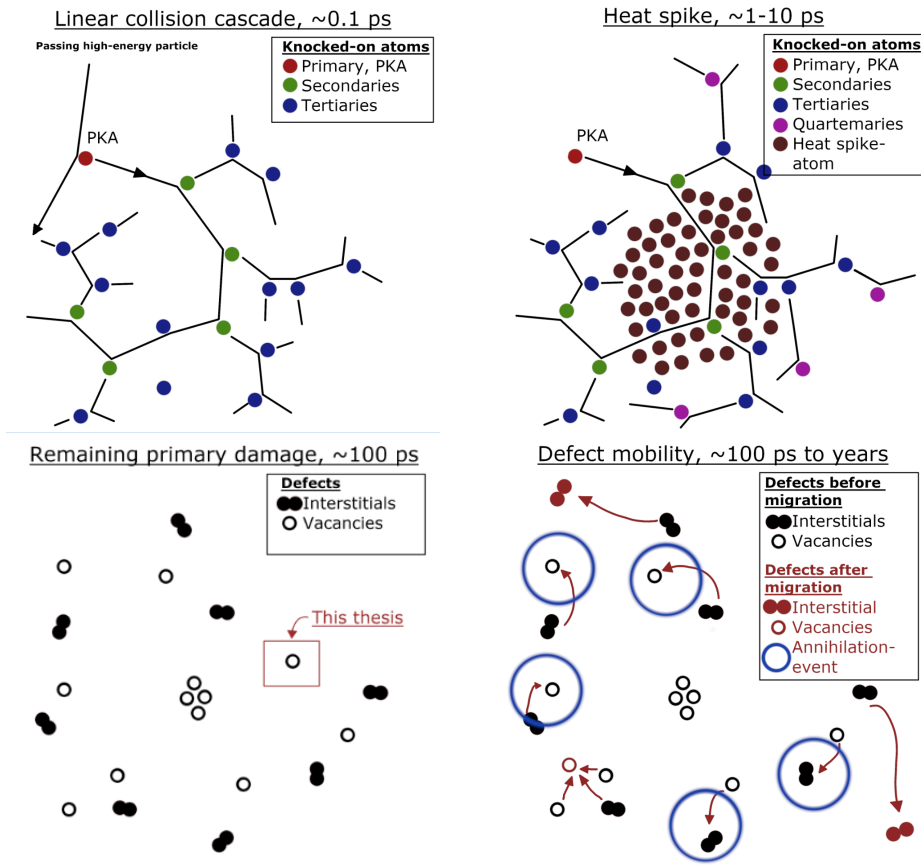


Figure 1.2: Shows the trajectory of the PKA and the secondary and tertiary knock-on particles, the thermal spike occurring in mid-event and the remaining point defects when the PKA has come to rest. The lower right image shows the annihilation process. [5]

Based on this model; Norgett, Robinson and Torrens developed a model [7] that includes inelastic collisions with electrons, and crystallographic directions for the TDE which forms a more general model of the number of point defects generated in the radiation damage event. This model is referred to as the Norgett-Robinson-Torrens (NRT) model and the number of point defects generated by the PKA is given by:

$$v_{\text{NRT}}(T) = \kappa \frac{T_{\text{dam}}}{2\langle T_{\text{tde}} \rangle} \quad (1.2)$$

where κ is the displacement efficiency and T_{dam} is the elastic component of T. $\langle T_{\text{tde}} \rangle$ is the mean value of the TDE over all crystallographic directions.

CHAPTER 1. INTRODUCTION

The NRT model is useful for calculating the displacements per atom (dpa), which is a useful unit in research of irradiated metals [8, 9, 10]. It is achieved by normalizing the NRT value with the total number of atoms, which will yield a unitless expression for the concentration of displaced atoms in a material volume [11].

Thermal spike

The radiation damage affects the material in a three-dimensional region in which the point defects perturb its density (this event can be viewed in figure 1.3). In comparison to the equilibrium density, the region of the cluster is dense in its outer rim as a result of the local increase in self-interstitial atoms, and simultaneously sparse in the vacancy-rich area. The affected region as a whole is referred to as a thermal spike (or sometimes heat spike) due to the fact that the average kinetic energy of the atoms compares to a temperature in the range of 10 000K.

This happens in a time-interval of tens of picoseconds and the local aggregation state of the material could potentially be considered liquid or even gaseous. The energy is relaxed in the same range of time as it was built up [13]. During this time, the high temperature and high diffusion rates permit most of the vacancies and SIA's to annihilate, which is shown in figure 1.2, or simply diffuse to a stable location which could be described as a form of local recrystallization. At the end of the radiation damage event, there will be only a few point defects left that have not yet reformed, which will thus be the residual effect of the whole event [14].

Effects on microstructure and mechanical properties

The radiation damage event has subsequent effects on the physical properties of the material. The most direct consequences are radiation-induced segregation, phase-changes, swelling, hardening, embrittlement and degradation of thermal transport properties, which will briefly be concluded in order of appearance in this text.

The rearrangement of atoms during the radiation damage event can cause concentration differences of the alloying elements. Due to the different mobility of the various atom species, the mobile atoms may relocate and form an enriched region, whereby the adjacent region will be depleted. This radiation-induced segregation tends to occur in regions near structural extremities e.g.

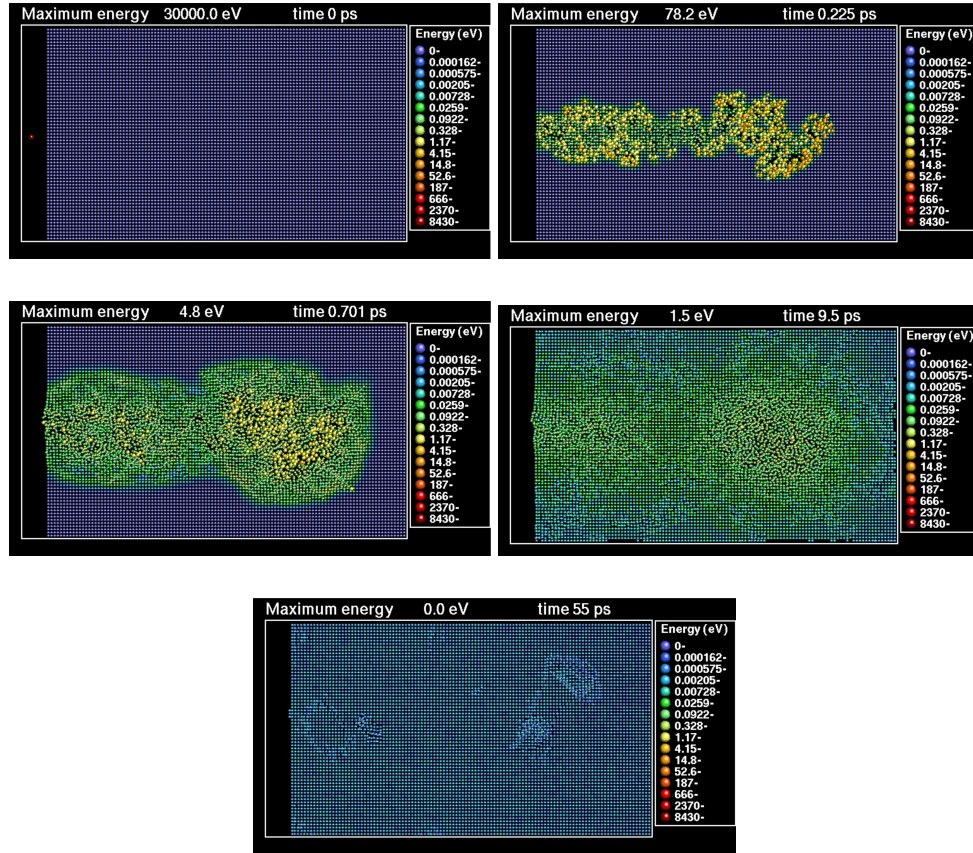


Figure 1.3: The collision cascade event simulated by use of molecular dynamics. It shows the thermal spike and the following energy distribution over a time interval of 55ps (public domain images made by Kai Nordlund [12]).

near grain boundaries, dislocations, or the surface of the material. By altering the concentrations of the present atom species in the microstructure, phase-changes can also take place where precipitates may form if the solubility limit is exceeded in the enriched regions, or preceded in the depleted regions. The radiation-induced segregation and phase-changes are more common at higher temperatures since they are governed by the mobility of the atoms and thus the diffusion rate, which increases exponentially with temperature.

As stated earlier, vacancies will form due to irradiation of the material and if the vacancy concentration rises above the saturation limit, i.e. the vacancies becomes supersaturated, a driving force will emerge for the vacancies to agglomerate and thus create voids and bubbles. Void and bubble formation

CHAPTER 1. INTRODUCTION

are two separate phenomena that are somewhat similar. The main difference is that voids are an agglomeration of vacancies whereas the bubbles are voids that contain inert gaseous particles, often a product from the nuclear reaction process. Voids and bubbles significantly affect the properties of the material in several ways. They may cause the material to swell, meaning that the volume may increase by tens of percent. They may also act as crack initiation points which makes brittle fractures more apparent.

Irradiation has a significant effect on the mechanical properties. A set of stress-strain curves of body-centered cubic (BCC) and face-centered cubic (FCC) steel are shown in figure 1.4 at different doses of irradiation.

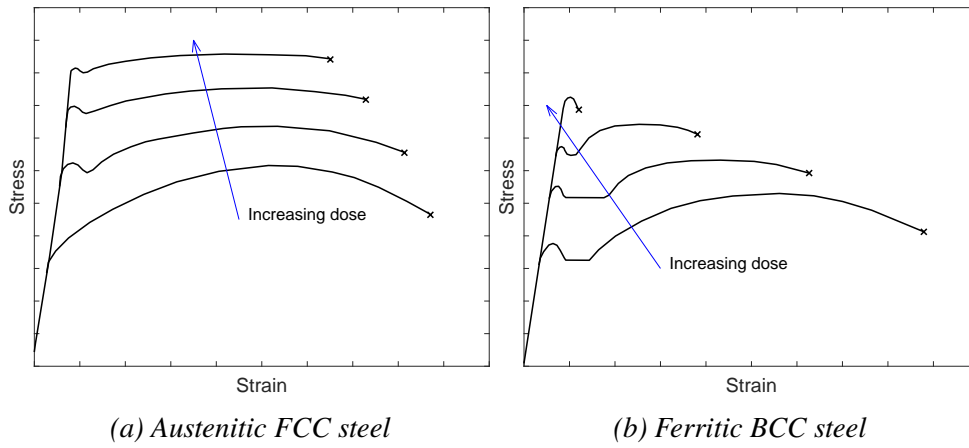


Figure 1.4: Irradiation effects on the stress-strain curve of a (a) FCC stainless steel and (b) BCC steel [15].

Uniform for both materials are that the yield stress, (σ_y), and ultimate tensile stress, (σ_{UTS}), increases with increasing irradiation dose. This is due to the point-, line-, and bulk defects that are formed in the microstructure as a result of the radiation damage. The defects act as obstacles for any dislocations to glide freely in the lattices and thus hardens the material.

The Young's modulus remains constant, but the ductility is degraded for the ferritic BCC steel, showing that the irradiation severely embrittles the steel. The major mechanism for this behavior is the segregation dependent precipitates that form as a consequence of irradiation. It is believed that the formation of phosphorous phases is the most harmful for the material [16, 17].

It is known that materials under stress in elevated temperatures will experi-

ence creep, i.e. slowly deform plastically over time. Creep is dependent on stress and temperature, and the creep rate will increase with increased stress and temperature. The radiation damage event usually has little effect on the creep mechanism, shown by Ghosh et.al. [18], but the creep rate is affected by the absorbed dose of radiation. The irradiation creep rate is a well-studied topic and many experiments have been conducted throughout history [19, 20]. The phenomenon is often described by equation 1.3 which was developed by Foster et.al. in 1972 [21]. This general equation describes the irradiation creep rate, $\dot{\epsilon}$, as a function of dpa:

$$\frac{\dot{\epsilon}}{\sigma} = B_0 + D\dot{S} \quad (1.3)$$

where σ is the applied stress, B_0 the creep compliance, D is the creep-swelling coupling coefficient, and \dot{S} is the dpa dependent swelling-rate. Irradiation creep is most significant at lower temperatures in the range of approximately $0.2-0.45T_{\text{melt}}$, where the thermal creep rate is still inhibited by the low diffusion rates [22]. In this temperature region, irradiation creep can magnify the creep deformation rate by orders of magnitude higher than for thermal creep alone since the radiation-induced supersaturation of defects greatly enhances diffusion in the lattice. However, for higher temperatures, thermal creep tend to take over which can be reviewed in figure 1.5.

1.1.2 Thermal transport and Phonons

For macroscopic investigation on thermal conductivity (κ), Fourier's law is applicable and describes the diffusive heat transport in the material. But in order to study the radiation damage effects on an atomic length scale, scattering effects will be dominant and Fourier's law will be insufficient. The *ab initio* transfer of heat energy in metals is more favorably described by a combination of two separate mechanisms where the first being electron thermal conductivity, κ_e , which is energy transport via electrons. And the second one being lattice thermal conductivity (LTC), κ_l , which is transport through inter-atomic vibrations. The two contributions do not generally interfere with one another, they simply sum up as the total thermal conductivity:

$$\kappa = \kappa_l + \kappa_e \quad (1.4)$$

The electrons contribute to heat transport by the induced diffusion of heat energy amongst the electrons due to a thermal gradient. It is comparable to the electrical conductivity according to the Wiedemann-Franz law which states

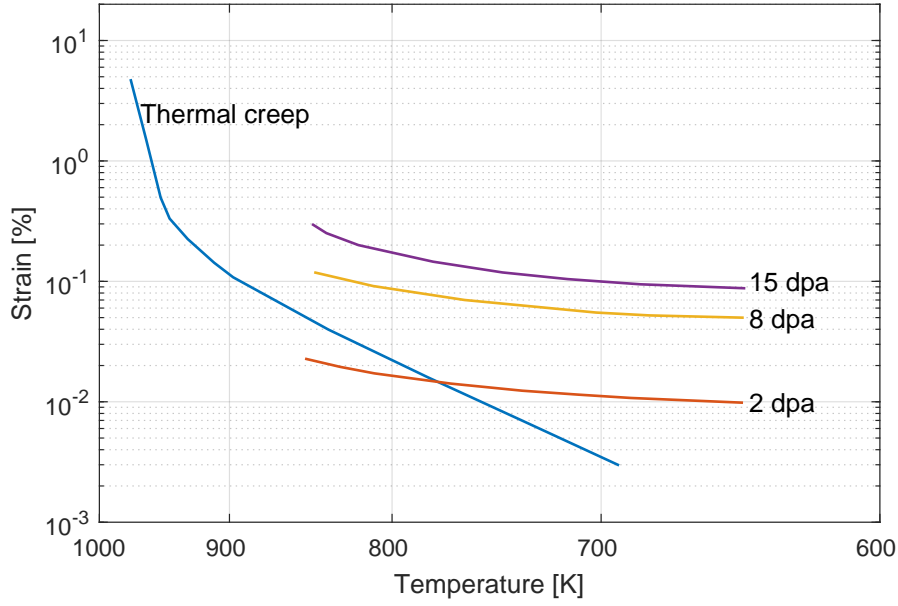


Figure 1.5: A schematic graph over the effect of irradiation creep on the total creep rate. The experiment is performed on a cold-worked stainless steel by E. Gilbert and J. Bates in 1977 [23].

that the relation between the thermal and electrical conductivity (σ) is proportional to the temperature [24]:

$$\kappa_e = LT\sigma \quad (1.5)$$

where L is a proportionality factor known as the Lorenz number.

Lattice thermal conductivity

As stated earlier, the lattice thermal conductivity is the transport of vibrations in the lattice, where the atoms reach excited vibrational states which spread to neighboring atoms. These excitations are known as phonons. When considering lattice thermal conductivity, phonons are preferably viewed as pseudo-particles containing discrete wave packets in the same manner that photons are described in the wave-particle dualism, and the heat transfer corresponds to phonon particle propagation that counteracts the thermal gradient. The energy of the phonons is quantified in discrete steps as: $E = \hbar\omega$ where \hbar being the reduced Planck's constant and $\omega = \omega(k)$ is the angular frequency which depends on the wave vector k .

The phonons are classified in normal modes which correspond to their specific

vibration frequency and can be separated into acoustic and optical modes. The phonons in the acoustic mode will have its neighboring atoms oscillating in phase and the same direction as the regarded atom. And in the Gamma point, i.e. center of the Brillouin zone, the frequency will be zero: $k \rightarrow 0 \implies \omega \rightarrow 0$. The optical modes have their neighboring atoms move in the opposite direction and will have a finite value in the Gamma point. Both acoustic and optical waves have longitudinal and transverse wave counterparts. The optical and acoustic wave modes can schematically be seen in figure 1.6.

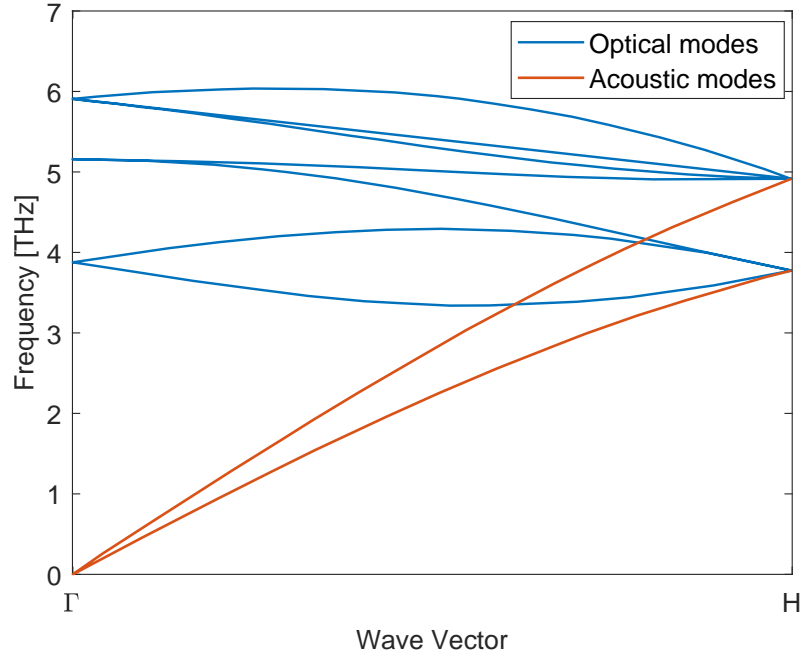


Figure 1.6: Optical and Acoustic wave modes

To derive a schematic expression for the point defects effect on the lattice thermal conductivity, one begins with the equation for the lattice thermal conductivity which can be written as:

$$\kappa_l = \frac{1}{3} \sum_{\mu} C_{\mu} v_{\mu}^2 \tau_{\mu} \quad (1.6)$$

where C , v and τ corresponds to the lattice specific heat, the group velocity and the phonon lifetime which are summed over all phonon modes, μ . Now the mean free path between collisions, λ , can be described as the group velocity multiplied with the phonon lifetime: $\lambda = v\tau$ which is further summed over all

CHAPTER 1. INTRODUCTION

phonons as equation 1.7 to get the net mean free path.

$$\lambda = \frac{1}{\sum_i \frac{1}{\lambda_i}} \quad (1.7)$$

This will render the lattice thermal conductivity as:

$$\kappa_l = \frac{1}{3} C_V \langle v \lambda \rangle \quad (1.8)$$

where C_V is the isochoric heat capacity and the brackets indicate the average value over all phonon modes [25, 26].

We now see that the lattice thermal conductivity is directly dependent on the specific heat capacity, phonon group velocity, and their mean free path. The specific heat capacity is temperature-dependent and will partly be responsible for the change in lattice thermal conductivity resulting from the change in temperature, while the group velocity is dependent on the density of phonon modes and the inter-atomic bond strength. The mean free path is affected by all forms of lattice distortions (e.g. bulk-, line- and point defects) and phonon-phonon scattering which all severely shortens the mean free path.

There are two different types of phonon-phonon scattering: normal- and Umklapp scattering. In normal scattering, two phonons may collide which combines to a single phonon that preserves the crystal momentum and does not affect the lattice thermal conductivity. This type of scattering is only present at low temperatures where the phonons are sparsely distributed in the lattice. However, the Umklapp scattering is the scattering process when two colliding phonons are merging into a phonon with a wave vector that stretches beyond the first Brillouin zone into the second zone, and thus the resulting vector can be described as a vector in the opposite direction within the first Brillouin zone. The crystal momentum is not preserved in this case because of the translation between Brillouin zones, and consecutively the lattice thermal conductivity will be affected. The Umklapp scattering scales with temperature and is a significant contributor to the degradation of lattice thermal conductivity at elevated temperatures.

1.1.3 Boltzmann Transport Equation

Phonons are classed as bosons and thus, the arrangement of phonons in a system in equilibrium is described by the Bose-Einstein distribution (eq. 1.9)

which is a quantum-statistic expression on the distribution of phonons in a system in equilibrium.

$$n_{q\alpha}^0(\omega_{q\alpha}, T) = \frac{1}{e^{\hbar\omega_{q\alpha}/k_B T} - 1} \quad (1.9)$$

Here, $n_{q\alpha}^0$ is the number of phonons with wave vector q in branch α and angular frequency $\omega_{q\alpha}$ at equilibrium temperature, T . The reduced Planck's constant and Boltzmann's constant are denoted by \hbar and k_B respectively.

When the system deviates from equilibrium, the phonons will diverge from the Bose-Einstein distribution and their behavior can be described by the Boltzmann transport equation (BTE). The BTE was originally developed in 1872 by Ludwig Boltzmann in his study of the "kinetic theory of gases" as an attempt to describe the properties of dilute gases by analyzing the interactions between two colliding particles [27]. The equation concludes in a probability distribution for the said particles and ends up being broadly utilized in several applications.

The distribution of phonons ($\mathbf{n}_q = \mathbf{n}_q(\mathbf{r}, t)$) in the non-equilibrium system will change primarily due to diffusion caused by a thermal gradient which will account for a concentration gradient of phonons and secondarily by collision interactions amongst them. Hence, the total change in the distribution is described by:

$$\frac{\partial \mathbf{n}_q}{\partial t} = \left. \frac{\partial \mathbf{n}_q}{\partial t} \right|_{\text{drift}} + \left. \frac{\partial \mathbf{n}_q}{\partial t} \right|_{\text{collision}} \quad (1.10)$$

The distribution of the system in equilibrium will be constant with respect to time,

$$\frac{\partial \mathbf{n}_q}{\partial t} = 0 \quad (1.11)$$

and thus the total change in the distribution will become zero. This will render the BTE:

$$\left. \frac{\partial \mathbf{n}_q}{\partial t} \right|_{\text{drift}} = - \left. \frac{\partial \mathbf{n}_q}{\partial t} \right|_{\text{collision}} \quad (1.12)$$

The diffusion driven operator that is a functional of the change in distribution is fairly straight-forward and can generally be expanded as:

$$\left. \frac{\partial \mathbf{n}_q}{\partial t} \right|_{\text{drift}} \equiv \frac{\partial \mathbf{n}_q}{\partial t} + \mathbf{v}_q \frac{\partial \mathbf{n}_q}{\partial \mathbf{r}} + \mathbf{F}_q \frac{\partial \mathbf{n}_q}{\partial \mathbf{v}} \quad (1.13)$$

where \mathbf{v}_q denotes the velocity and \mathbf{F}_q is the external forces experienced by the particles. The term regarding the external forces is negligible in this case

since phonons can not be affected by any external forces. However, the crux in solving the BTE lies in the collision term, which is a non-linear integro-differential equation and is a rather difficult problem to solve. To grasp the complexity in resolving the collision term it will be viewed upon as the most standard example when two phonons, \mathbf{q} and \mathbf{q}' collides and forms a third phonon, \mathbf{q}'' . This would give the collision term the following form:

$$\left. \frac{\partial \mathbf{n}_{\mathbf{q}}}{\partial t} \right|_{\text{coll}} = \int \int \left(\mathbf{n}_{\mathbf{q}} \mathbf{n}_{\mathbf{q}'} (\mathbf{n}_{\mathbf{q}''} + 1) - \frac{1}{2} \mathbf{n}_{\mathbf{q}} (\mathbf{n}_{\mathbf{q}'} + 1) (\mathbf{n}_{\mathbf{q}''} + 1) \right) \Omega_{\mathbf{q}, \mathbf{q}', \mathbf{q}''} \frac{d\mathbf{q}' d\mathbf{q}''}{(2\pi)^3} \quad (1.14)$$

where $\Omega_{\mathbf{q}, \mathbf{q}', \mathbf{q}''}$ is the probability of the transformation of phonons \mathbf{q} and \mathbf{q}' to the adaptive phonon \mathbf{q}'' from the collision. This example will continue with in equation 1.17 with the linearized form of the BTE.

Linearized Boltzmann transport equation

For systems that does not concern large deviations from equilibrium, the BTE can be linearized by using the equilibrium distribution with a deviation term which will form the linearized Boltzmann transport equation (LBTE):

$$\mathbf{n}_{\mathbf{q}} = \mathbf{n}_{\mathbf{q}}^0 + \delta \mathbf{n}_{\mathbf{q}} \quad (1.15)$$

and if the only deviation in the system is assumed being the temperature gradient, ∇T , the deviation term, $\delta \mathbf{n}_{\mathbf{q}}$, is expanded as [28]:

$$\delta \mathbf{n}_{\mathbf{q}} = \frac{\partial \mathbf{n}_{\mathbf{q}}}{\partial \epsilon_{\mathbf{q}}} \cdot \frac{\partial \epsilon_{\mathbf{q}}}{\partial A} \nabla T \cdot \Delta \mathbf{r} = \frac{\partial \mathbf{n}_{\mathbf{q}}}{\partial \epsilon_{\mathbf{q}}} \Phi_{\mathbf{q}} = \frac{\mathbf{n}_{\mathbf{q}}^0 (\mathbf{n}_{\mathbf{q}}^0 + 1)}{k_B T} \Phi_{\mathbf{q}} \quad (1.16)$$

where $\mathbf{n}_{\mathbf{q}}^0$ refers to the equilibrium distribution and $\Phi_{\mathbf{q}}$ represents the total deviation from equilibrium.

To continue the example with the three phonons by using equation 1.15 and 1.16 in the collision operator (equation 1.14), the following expression is retrieved:

$$\left. \frac{\partial \mathbf{n}_{\mathbf{q}}}{\partial t} \right|_{\text{collision}} = \int \int (\Phi_{\mathbf{q}} - \Phi_{\mathbf{q}'} - \Phi_{\mathbf{q}''}) P_{\mathbf{q}, \mathbf{q}', \mathbf{q}''} \frac{d\mathbf{q}' d\mathbf{q}''}{(2\pi)^3} \quad (1.17)$$

where $P_{\mathbf{q}, \mathbf{q}', \mathbf{q}''}$ is a term for the rate of the transformation process. And as a clarification, this example is not a complete derivation of the problem, it simply acts as a mathematical tool for better understanding the process.

With the BTE in a linearized form, the collision- and drift operator can be expressed as matrices functioning on the phonon distribution as in equation 1.12, and one achieves the following equation:

$$\mathbf{C}\mathbf{n} = \mathbf{D}\mathbf{n} \quad (1.18)$$

where \mathbf{C} and \mathbf{D} corresponds to the collision and the drift operator respectively. Now the problem becomes a search for eigenfunctions to the operator matrices. This is still a profound challenge to solve analytically, and requires further simplifications. Several methods have been developed over the years for approaching this problem. Amongst those are the relaxation time approximation (RTA) which will be briefly assessed.

Relaxation time approximation

The assumption that is made in RTA is that the relaxation time for the excited phonon to return to its equilibrium state is not dependent of other excited phonon collisions, only collisions with phonons in equilibrium. This would transfer to the example as $\mathbf{n}_{\mathbf{q}'} = \mathbf{n}_{\mathbf{q}'}^0$ and $\mathbf{n}_{\mathbf{q}''} = \mathbf{n}_{\mathbf{q}''}^0$, meanwhile equation 1.15 is still useful. With these assumptions, the BTE can be described functioning on the relaxation time, $\tau_{\mathbf{q}}$, as:

$$v_{\mathbf{q}} \nabla \mathbf{n}_{\mathbf{q}}^0 = - \frac{\mathbf{n}_{\mathbf{q}} - \mathbf{n}_{\mathbf{q}}^0}{\tau_{\mathbf{q}}} \quad (1.19)$$

with the phonon group velocity, $v_{\mathbf{q}}$, and the relaxation time, which can be expressed as:

$$\frac{1}{\tau_{\mathbf{q}}} = \Phi_{\mathbf{q}} \int \int \mathbf{P}_{\mathbf{q},\mathbf{q}',\mathbf{q}''} \frac{d\mathbf{q}' d\mathbf{q}''}{(2\pi)^3} \quad (1.20)$$

This equation is solvable without much effort and by applying thermodynamic descriptions of heat flux, the lattice thermal conductivity can be obtained:

$$\kappa_l = \int C_{\mu} v_{\mathbf{q}}^2 \tau_{\mathbf{q}} D(\omega) d\omega \quad (1.21)$$

where C_{μ} is the specific heat of the phonon mode, μ , and $D(\omega)$ is the density of states (DOS) [29, 30, 31]. Make sure to note the similarity with equation 1.6.

1.1.4 Density Functional Theory

To be able to perform simulations on quantum mechanic determined systems, one needs to address the Schrödinger equation which is the key to unlock the

CHAPTER 1. INTRODUCTION

enigma of quantum mechanics. As of the last 40 years, the most used method to solve the Schrödinger equation (Eq. 1.22) is by Density Functional Theory (DFT) which is also used in this thesis. It is more safe to say that DFT does not explicitly solve the Schrödinger equation, it rather uses a set of approximations which will be briefly described in this section. The Schrödinger equation contains the wave function, Ψ , which is a functional of the electron position, \mathbf{r}_i . And now the time-independent many-body Schrödinger equation, which is of interest in this thesis, is written:

$$\hat{H}\Psi(\mathbf{r}_1, \mathbf{r}_2, \dots) = E\Psi(\mathbf{r}_1, \mathbf{r}_2, \dots) \quad (1.22)$$

where the Hamiltonian operator, \hat{H} , is a functional of Ψ , and can be separated into three terms as of:

$$\hat{H} = T + V_{ee} + V_{ext} \quad (1.23)$$

where T is the kinetic energy, V_{ee} the interactions between electrons, and V_{ext} the external potential, which in this material-related thesis will correspond to the interactions between electrons and ions in the crystal structure. The Hamiltonian operator on each term in equation 1.23 is expanded as:

$$\hat{H} = -\frac{\hbar^2}{2m_i} \sum_i \nabla_i^2 + \sum_i \sum_{j>i} V_{ee}(\mathbf{r}_i, \mathbf{r}_j) - \sum_i V_{ext}(\mathbf{r}_i) \quad (1.24)$$

where each term corresponds to their respective term in equation 1.23. Note that the spin properties of the electrons will be excluded in this report because the subjected atom is tungsten, which has four valence atoms in separate orbits, thus the electron spin polarization can be neglected.

The movement of the electrons and ions can be separated from one another. This is described mathematically as:

$$\Psi(\mathbf{R}_i, \mathbf{r}_i) = \Psi(\mathbf{R}_i)\Psi(\mathbf{r}_i) \quad (1.25)$$

and is an approximation derived by Max Born and Robert Oppenheimer in 1927 [32]. It states that since the masses of the ionic nuclei are significantly higher than that of the electrons, and because the difference in velocity is thus scaling by several orders of magnitude, the electrons are considered to move in a space of fixed ions. This can be objectively described by classic mechanics where one can consider to compare the momentum of each particle via:

$$\mathbf{p} = m \cdot \mathbf{v} \quad (1.26)$$

where \mathbf{p} is the momentum of the particle with mass, m , and velocity, \mathbf{v} . The masses of the electrons and ions are considered fixed and that leaves the velocity as the only variable which will account for the difference in magnitude. To

find the ground-state energy of the system, the energy term in equation 1.22 needs to be minimized by finding the particular Ψ that does this in:

$$E[\Psi] = \int \Psi^* \bar{H} \Psi d\mathbf{r} \equiv \langle \Psi | \bar{H} | \Psi \rangle \quad (1.27)$$

and this Ψ can not transcend below the absolute ground-state energy E_0 according to the variational principle (Eq. 1.28).

$$E[\Psi] \geq E_0 \quad (1.28)$$

The practical complexity for solving the Schrödinger equation escalates quickly since the dimensions of the problem scales by three times the number of electrons, N . For example, Tungsten has 74 electrons and a cluster of 54 atoms would result in a near 12000 dimensional highly correlated problem, which would require more computational power than what currently exists on the planet.

The Hohenberg-Kohn theorems

In 1964, Hohenberg and Kohn presented two groundbreaking theorems, which they in the year 1998 achieved the Nobel price for [33]:

Theorem 1 The ground state of a many-body system with inter-particle interactions is a unique functional of the electron density, $E = E[\rho(r)]$, where $\rho(r)$ is the electron density.

Theorem 2 The electron density that minimizes the total energy functional $E[\Psi]$, with the condition that $\int \rho(\mathbf{r}) d\mathbf{r} = N$, is the true electron density of the system.

This significantly reduces the complexity of the problem and allows equation 1.23 to be determined by the electron density rather than the interactions between each and every electron in the system. This means that from the example stated earlier, the dimensions would reduce from near 12000 to only three dimensions for the single electron. However, the theorems do not state what the functional actually is, only that it does exist. So, if one were to find the true electron density of the system it would be possible to determine the ground state energy. With these theorems applied to the Schrödinger equation, the energy functional can be expressed in terms of electron density in the same form as equation 1.23:

$$E[\rho(\mathbf{r})] = T[\rho(\mathbf{r})] + V_{ee}[\rho(\mathbf{r})] + V_{ext}[\rho(\mathbf{r})] \quad (1.29)$$

Kohn-Sham equations

To progress in solving the Schrödinger equation, Kohn and Sham proposed in year 1965 a method for solving the associated energy functional by simplifying the kinetic energy term and electron interaction term while introducing a new term accounting for the simplifications [34]. Equation 1.29 evolves to:

$$E[\rho(\mathbf{r})] = T_s[\rho(\mathbf{r})] + V_H[\rho(\mathbf{r})] + V_{\text{ext}}[\rho(\mathbf{r})] + E_{\text{XC}}[\rho(\mathbf{r})] \quad (1.30)$$

presuming that $T_s[n(\mathbf{r})]$ is the non-interacting kinetic energy of the system which defines it as the product of the orbital densities as:

$$T_s[\rho(\mathbf{r})] = -\frac{1}{2} \sum_i^N \langle \phi_i | \nabla^2 | \phi_i \rangle \quad (1.31)$$

where ϕ_i is the specified orbital, thus the ground state density will be:

$$n(\mathbf{r}) = \sum_i^N |\phi_i|^2 \quad (1.32)$$

As stated earlier, the term V_{ext} accounts for the electron-nuclei interaction and is addressed as the external potential. It is described mathematically as:

$$V_{\text{ext}}[\rho(\mathbf{r})] = \int \hat{V}_{\text{ext}} \rho(\mathbf{r}) d\mathbf{r} \quad (1.33)$$

The term V_{ee} in equation 1.29 is describing the single electrons Coulomb interactions with the electron density meanwhile the single electron is included in the electron density. This means that the electron is interacting with itself, which is a flaw in the calculations and is accounted for in the correction term, E_{XC} [35]. The now correlated electron-electron interaction term consists of classical Coulomb interactions with the density and can be defined as a Hartree energy potential:

$$V_H[\rho(\mathbf{r})] = \frac{1}{2} \int \frac{\rho(\mathbf{r}_1)\rho(\mathbf{r}_2)}{|\mathbf{r}_1 - \mathbf{r}_2|} d\mathbf{r}_1 d\mathbf{r}_2 \quad (1.34)$$

Now the energy functional is defined in equation 1.29 with the only unknown term being the exchange correlation energy:

$$E_{\text{XC}}[\rho(\mathbf{r})] = (T[\rho(\mathbf{r})] - T_s[\rho(\mathbf{r})]) + (V_{\text{ee}}[\rho(\mathbf{r})] - V_H[\rho(\mathbf{r})]) \quad (1.35)$$

which accounts for the flaws of using the classical approach on the electron-electron interaction and for using the non-interacting model of the kinetic energy.

Local density approximation

There are several approaches for computing E_{XC} , and one of the most widely used and also simpler methods is called Local Density Approximation (LDA). LDA is a set of approximations derived from the Thomas-Fermi homogeneous electron-gas (HEG) model in the 1920s [36] where the exchange-correlation energy, E_{XC} , is considered to depend solely on the local density of the electron-gas. Generally in LDA the total exchange-correlation energy is described as the integral of the exchange-correlation energy within every particle (ϵ_{xc}) as:

$$E_{XC}(\rho) = \int \rho(\mathbf{r}) \epsilon_{xc}(\rho(\mathbf{r})) d\mathbf{r} \quad (1.36)$$

and is also linearly separated in to two exchange and correlation terms respectively.

$$\epsilon_{xc} = \epsilon_x + \epsilon_c \quad (1.37)$$

It is achieved from the HEG model that ϵ_x is proportional to $\rho^{1/3}$ by a free constant while ϵ_c is unknown. However, several reports has utilized Monte-Carlo methods for calculating ϵ_c which have all yielded similar results [37, 38, 39]. The combined functional ϵ_{xc} has proven to be useful and is since referred to as the LDA functional.

Generalized gradient approximation

The LDA regards the electron density as being constant in all locations, which has a tendency to lead to errors where the energy in the correlation term tends to overwhelm the exchange term in equation 1.37. This is corrected in equation 1.35 by introducing the gradient of the electron density for the exchange-correlation energy as:

$$E_{XC}(\rho) = \int \rho(\mathbf{r}) \epsilon_{xc}(\rho(\mathbf{r}), \nabla \rho(\mathbf{r})) d\mathbf{r} \quad (1.38)$$

which improves the already accurate results from LDA. This is called the generalized gradient approximation (GGA) and is one of the most commonly used methods for approximating the exchange-correlation term.

1.1.5 Vienna Ab-Initio Simulation Package

Vienna Ab-Initio Simulation Package (VASP) is a computer program developed by Georg Kresse and his colleagues [40, 41], made for modeling materials based on first-principle methods. It uses the DFT method for computing

CHAPTER 1. INTRODUCTION

approximate solutions to the many-body Schrödinger equation (eq. 1.22) i.e. determine the ground state energy of the electrons. But as of today, more advanced methods are also implemented in VASP for more accurate models.

VASP requires four different input files to be able to conduct the calculations. the first file containing the pseudo-potential for the specific element. A second file for setting up the basis orientations of the lattice where the amount of atoms, positions, and lattice spacing is determined. This is the basis for the model and the boundary conditions is set according to these parameters. The third file describes the resolution of the Brillouin zone and how the program will render it. And the fourth file concludes all the specifications for the model and tells VASP how the simulation should be made.

In this work, VASP uses the projector-augmented wave potential (PAW) [42] to compute the electron-ion interactions which are expressed in plane-wave basis sets. VASP uses a very efficient iterative process for reaching the ground state, which makes it very effective in the use of computer power.

When using VASP it is often more beneficial to work in the reciprocal space than in real space. To render the reciprocal space in VASP, the term k-points is used which refers to the resolution that the first Brillouin zone is rendered in. Here, a N^3 number of k-points would refer to the division of the first Brillouin zone into a $NxNxN$ grid of k-points, where the dimension of k is of inverse length:

$$k = \frac{n2\pi}{L} \quad (1.39)$$

where n is an integer and L is the length of the crystal in one direction. Note that the value of L will determine the number of k-points needed for executing accurate simulations where a larger crystal will need fewer k-points to return accurate simulations.

1.1.6 Phono3py

This is a software developed by Atsushi Togo [43] which uses a supercell approach to calculate the phonon-phonon interactions in a crystal lattice. From these calculations, several physical properties can be obtained, e.g. lattice thermal conductivity and the phonon lifetime. The calculations are made by using either the RTA method or a direct solution to solve the LBTE. Phono3py generates a set of displaced supercells where another independent computer

program needs to be applied to make DFT calculations in order to calculate the forces. The displacements in the supercells cause anharmonicity in the lattice which is needed for phonons and other thermodynamical phenomena to be present. The force calculations made on the displaced supercells are accumulated in phono3py which it uses to calculate the desired properties.

1.1.7 Phonopy

In addition to phono3py, another software is used which is also developed by Atsushi Togo. Phonopy [44] is a software for phonon calculations and it is used in this work to calculate the phonon band structure and density of states (DOS). It can be used to retrieve additional thermodynamic properties but this is not utilized in this thesis. The work-flow for phonopy is identical to phono3py in that a separate force calculator is needed.

Chapter 2

Methods

This thesis uses computational methods for conducting research on the topic and the chosen software for these simulations is VASP. And since computers use numerical, discrete values over finite intervals for making the calculations, and because the time usage scales with the number of data points, it is of utmost importance that the initiating values are set properly. This is because the aim is to get as accurate results on as low computer time usage as possible. When performing simulations of a new system in VASP, convergence testing needs to be made to define some fundamental parameters and to make sure the model is working properly.

Throughout the report, the PAW-PBE potential is used for Tungsten with an energy cut-off value set to 400 eV for the plane-wave basis set. Calculations are made using non spin-polarization and first-order Methfessel-Paxton smearing of the electron waves with the default smearing width of 0.2 eV. The reciprocal grid is centered around the Γ -point (Gamma (0 0 0)) and the number of k-points is set to $11 \times 11 \times 11$ if not stated otherwise.

2.1 Convergence tests

In this context, convergence testing is the iterative process of refining parameters to achieve a converged result in the calculations where successively increased precision is desired. There are a vast amount of parameters to adjust in VASP, in which most are left at the default setting and should not be altered unless the experiment requires it to be changed. In this thesis, the lattice parameter, energy cutoff parameter, vacancy formation energy and the lattice thermal conductivity are subjected to convergence tests.

2.1.1 Lattice parameter

In order to perform accurate simulations and to achieve proper interactions in the models, the lattice parameter needs to be defined as accurate as possible. To construct this value, a perfect crystal is simulated in VASP with the cell volume set as a degree-of-freedom, while the shape and atomic positions are locked. This will allow the atoms to move respective to one another to settle at the most stable spacing. A relaxation simulation is initiated with a starting estimation of the lattice parameter. While consecutively updating the lattice parameter and letting the system relax once again, the system will converge to the most stable value for the lattice parameter. For more complete accuracy, this method is iterated while having finer spacing of the integral paths in the reciprocal space (k-points) until the error is minimized.

2.1.2 Energy cut-off parameter

The basis-set of the system is built up by a set of plane waves which contains different amounts of energy. The plane waves that contain low amounts of energy generally contributes to a large effect in the total energy of the system, while the more energetic plane waves have smaller effect. VASP uses a parameter for limiting the amount of plane waves included in each basis set by excluding the plane waves that contain a higher kinetic energy than the limit is set to be. This is a way of optimizing the computer time usage against the preferred precision of the simulations. The PAW-PBE potential that are used in this thesis has a preset energy cut-off value which is manually altered to tailor the precision of the simulations. To establish a suitable value for the energy cut-off parameter, a convergence test is made similar to the previous one of the lattice parameter. But instead of varying the k-points, the cut-off energy is varied to set what cut-off energy is needed for the lattice parameter to converge.

2.1.3 Vacancy formation energy

The presence of vacancies in a lattice will hinder the system from reaching equilibrium by introducing asymmetry in the lattice and thus asymmetrical forces will occur. Ultimately, these asymmetrical forces result in a higher total energy of the system which can be measured, and by equation 2.1 a value for the rise in total energy caused by a single vacancy can be achieved.

$$E_{\text{form}}^{\text{vac}} = E_{\text{tot}}^{\text{vac}} - \frac{N_0 - 1}{N_0} E_{\text{tot}}^{\text{ref}} \quad (2.1)$$

Here, $E_{\text{form}}^{\text{vac}}$ is the vacancy formation energy, $E_{\text{tot}}^{\text{vac}}$ is the total energy of the supercell containing a vacancy and $E_{\text{tot}}^{\text{ref}}$ being the total energy of a perfect supercell with N_0 number of atoms. A perfect supercell in this context refers to a cell with no point defects. Here, a perfect supercell containing 54 atoms is simulated in VASP with conditions that the cell volume is constant and the atoms positions is free to move. The same settings is made for a supercell containing 53 atoms with the central atom removed. This will act as a vacancy, and the VASP simulations will let the system relax to find equilibrium. The total energy calculations returned from the simulations are used in equation 2.1 which in turn yields the vacancy formation energy.

2.1.4 Lattice thermal conductivity

In this thesis, phono3py is used to calculate the LTC which uses the force calculations performed by VASP on a set of displaced cells to achieve the results. The resulting LTC is thus highly dependent on the accuracy of the VASP simulations, it is in fact the most important aspect of the entire simulation. These simulations all regard a supercell of 16 Tungsten-atoms in BCC structure.

VASP parameters

Several parameters are investigated in VASP to bring more accurate results. For the force calculations in VASP, the following parameters are compared to see any effects in the accuracy:

- K-Points
- Energy cut-off
- Minimum energy difference
- Smearing method

The k-points are investigated separately by utilizing a convergence test. In this test, five calculations of the LTC is plotted with different settings for the number of k-points. The results of this simulation can be viewed in figure 3.4. In addition, the cut-off energy, minimum energy difference and the smearing method is investigated in figure 3.5

Phono3py parameters

Although phono3py is oriented to a specific task, it is a versatile program and many parameters can be adjusted to fit the problem under investigation. One parameter that is experimented with in this project is the second order force constant (fc2) option. Phono3py regularly uses the DFT calculations on the third-order force constants (fc3) to describe the phonon interactions in the system. Generally, this is very sensitive to perturbations that may be included in the force calculations, and can as a consequence return inaccurate values. This can be complemented by introducing a larger supercell in which only the second order force constants are calculated. However, it implies in this case that the DFT calculations that are first made on 16 atoms will now have to be made on 128 atoms, which is a very time-consuming process. In order to view the effects on the LTC by adding fc2 (figure 3.6), the simulations are made with lower number of k-points.

2.2 Effects of a vacancy

This section reviews the methods that has been used to evaluate the effects of a vacancy in a supercell of 16 atoms. Generally, the comparisons are made on two different models, where the only difference is the amount of atoms. The first model contains 16 atoms in a BCC structure with the lattice parameter set from the previous convergence test (figure 3.1). The second model has its central atom replaced by a vacancy, which is the only difference. In reality, the concentration of vacancies in a irradiated metal is rarely above the magnitude of one per million meanwhile in these models, a vacancy concentration of 1/16 is used, which is not close to realistic. However, the aim with these models is not to evaluate any numerical values but only to view the effects of one vacancy which is considered to be a feasible task.

2.2.1 Lattice thermal conductivity

In the first experiment of this section, the LTC is calculated over a temperature range from zero to 1000 degrees Kelvin in the two models. The settings that are used in the simulations are a result from the convergence test series. A number of displacements of the supercell is generated by phono3py which are each placed in separate folders. Each folder contains a supercell with some displacements, which are then subjected to force calculations in VASP. VASP creates a document containing all information gathered from the force calcu-

lation, and this document is assembled from all folders and put into phono3py. Now phono3py has received all information required for conducting calculations on the LTC.

2.2.2 Phonon band structure and density of states

The calculations the phonon band structure and density of states in phonopy follows the exact same method as for phono3py. For description of the phonopy methods, the reader is therefore directed to the previous subsection (2.2.1). The phonon band structure and total density of states is retrieved from the phonopy calculations.

Chapter 3

Results

In this chapter the results from the work will be divided in to two sections. The first section will display the convergence tests and resulting values compared with reference values from the literature. The aim with the simulations in this section is to confirm that the results are reliable and to tailor the altered parameters to their optimal settings.

The second section will regard all simulations that are aimed to compare the effects of vacancies in the supercell and are thus the goal-oriented results for this work. As stated in the previous chapter, the numerical results obtained in the simulations of this sections are not expected to coincide with reality. It is simply the differences that are of interest. In order for the numerical values to be more accurate, more computer power and more time is needed.

3.1 Convergence tests

Several convergence tests has been performed throughout this work and those results are presented in this section, where the effects of changing certain parameter values is studied. The conclusions made by studying these results are fundamental to the models in the next section because their parameter settings will be based on this investigation.

To make a clarification regarding some figures in this section, at the instances where the k-points are assigned to an integer N (e.g. in figure 3.1 and 3.3), it simply implies that the k-space is rendered in $N \times N \times N$ number of k-points.

3.1.1 Lattice parameter

This is the results from the convergence test on the lattice parameter of Tungsten. The values can be viewed in table 3.1 where the extracted value from figure 3.1 is compared with the reference value. The value achieved in the results are used for the remaining calculations in this report.

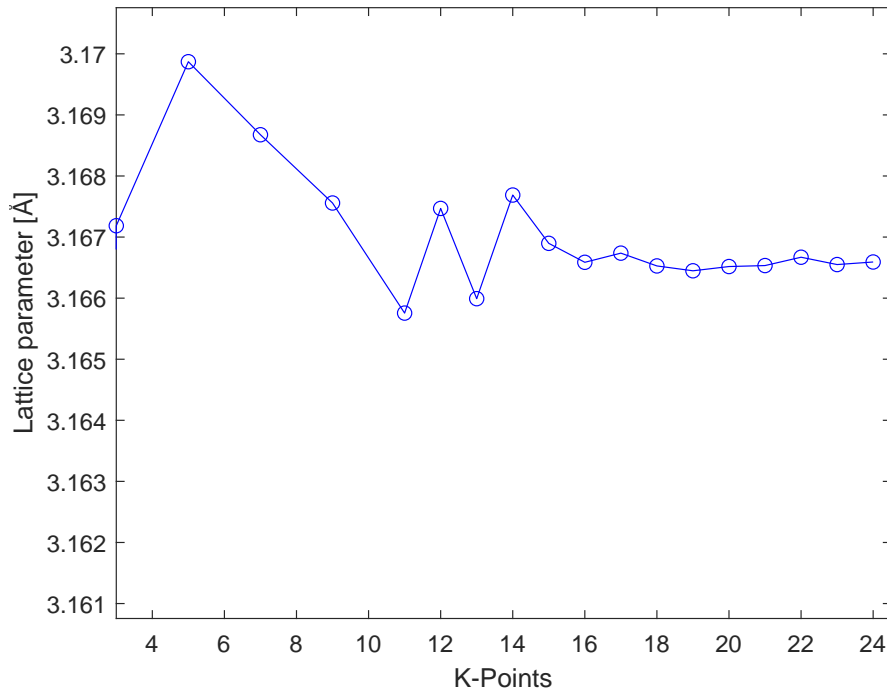


Figure 3.1: Relaxation of two Tungsten atoms at different spacing in the reciprocal grid. The lattice parameter is converging.

Table 3.1: Comparison between the calculated lattice parameter in this work and a reference value achieved from x-ray diffraction [45].

	Lattice parameter
This work	3.1666 Å
Reference	3.1652 Å

3.1.2 Energy cut-off parameter

The potential used in this experiment has a preset energy cut-off value at 223eV but a convergence test is made to act as a basis for determine what value for the cut-off energy that will be used further in the report. In figure 3.2 the lattice parameter converges over increasing value for the cut-off energy.

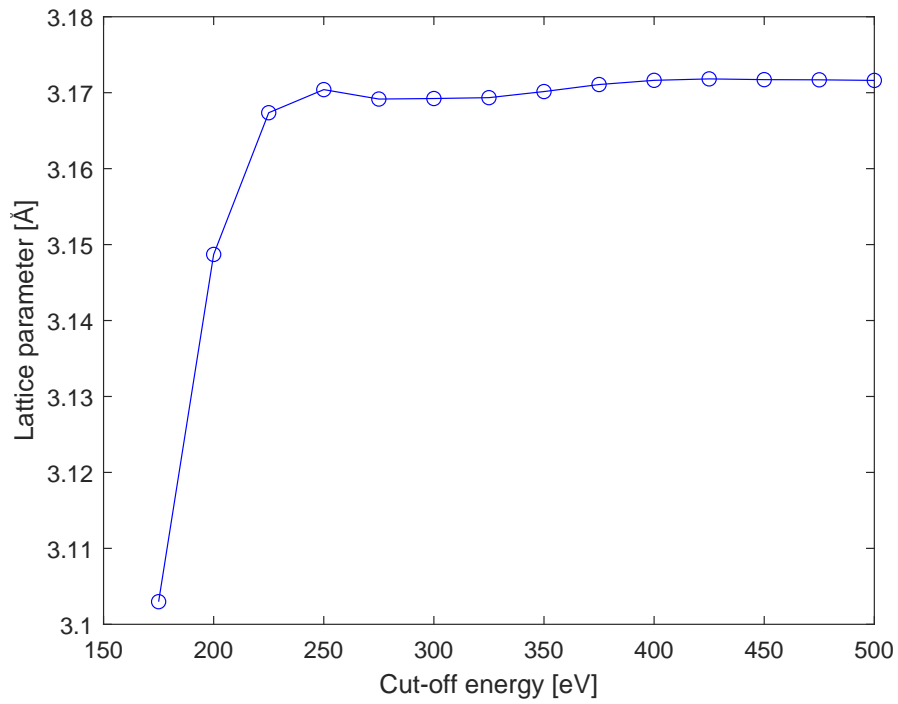


Figure 3.2: Convergence test of the energy cut-off parameter.

The curve in figure 3.2 reaches a plateau and is converging to a finite value of the lattice parameter. it is determined that a energy cut-off value of 350 eV is sufficient for the required precision throughout this report.

3.1.3 Vacancy formation energy

In this experiment the simulations are executed on 54 atoms which will limit the amount of k-points used because of the limitations in computer power. Figure 3.3 shows that the vacancy formation energy converges at 7x7x7 k-points.

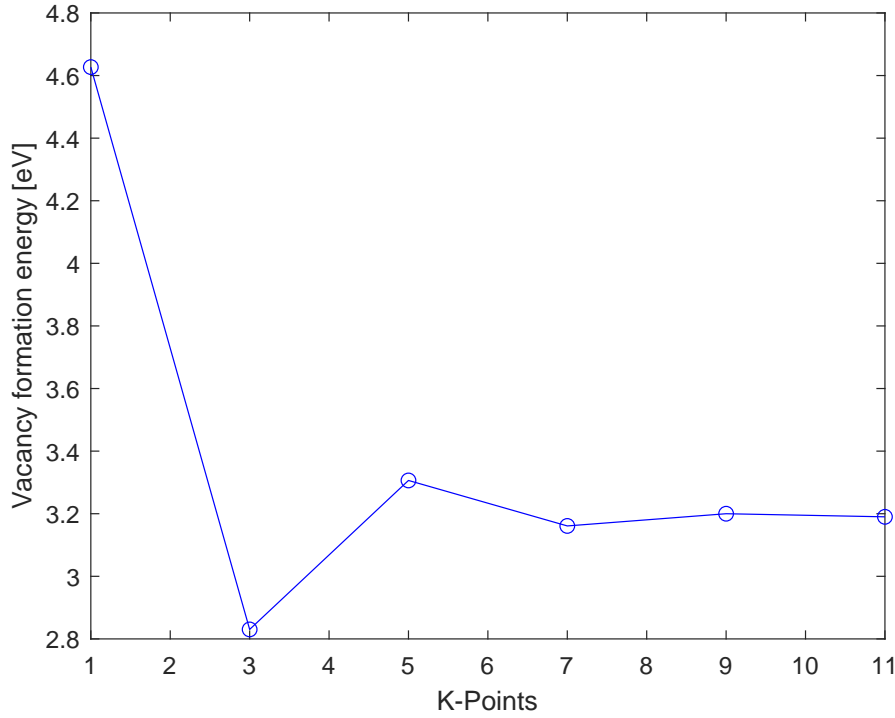


Figure 3.3: Vacancy formation energy converging over finer k-point grid

When comparing the point of convergence in figure 3.3 and 3.1, one notices a difference. This is explained by equation 1.39 where a larger cell requires fewer k-points to return accurate results.

Table 3.2: The vacancy formation energy ($E_{\text{form}}^{\text{vac}}$) calculated in this work compared to similar work conducted by Medasani *et.al.* using the PBE potential [46] and to specific heat experiments performed by Kraftmakher [47].

	This work	Other work	Experiment
$E_{\text{form}}^{\text{vac}}$	3.19 eV	3.31 eV	3.15 eV

3.1.4 Lattice thermal conductivity

Several attempts has been made to converge the lattice thermal conductivity closer to its reference value by refining certain parameters that affects the force calculations in both VASP and phono3py. The accuracy of the simulations conducted on the LTC is most easily reviewed by comparing the results against the LTC at room temperature found in the literature. At room temperature (300 K) the thermal conductivity is measured (by Laser Flash Method) to be 130 W/mK [48]. Note that this is the total thermal conductivity which includes the electron contribution. Beginning with refinement of the k-point grid which starts at a $3 \times 3 \times 3$ grid with iterative increase by two integers at a time to a $11 \times 11 \times 11$ grid yields the results presented in figure 3.4.

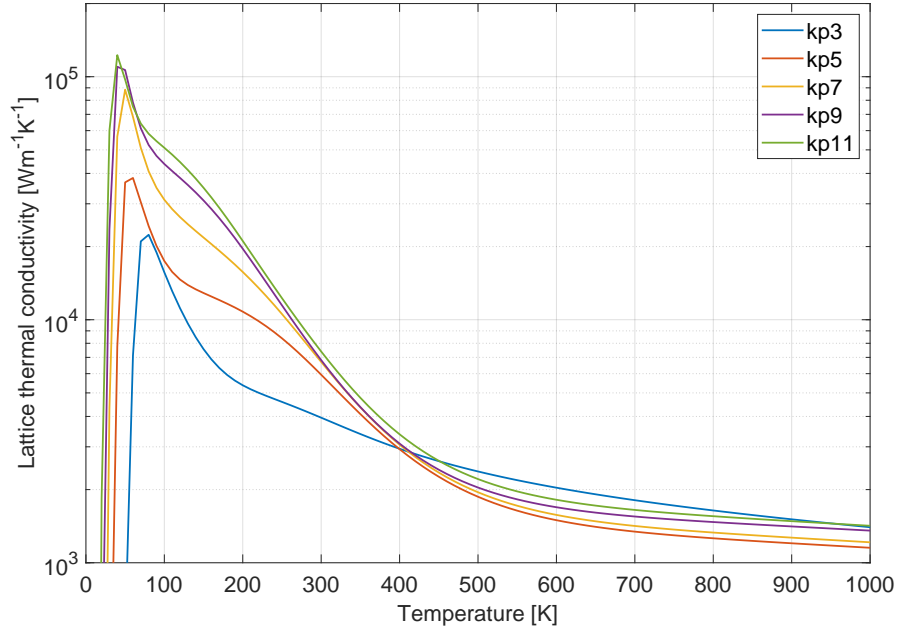


Figure 3.4: Lattice thermal conductivity as a function of temperature with different k-points (*kp N* refers to a $N \times N \times N$ grid).

The results in figure 3.4 seems to converge but the computer performance limits usage of increased k-points.

The energy cut-off parameter, minimum energy difference and the smearing method is investigated to reflect on their effect on the lattice thermal conductivity. The parameters of the models in figure 3.5 are set according to table 3.3 and the number of k-points are set to $11 \times 11 \times 11$ for the entire set of simulations.

CHAPTER 3. RESULTS

Table 3.3: Parameters for the simulations in figure 3.5

Model	Energy cut-off	Energy difference	Smearing
Reference	350	10^{-6}	Gaussian
Encut	400	10^{-6}	Gaussian
Ediff	350	10^{-8}	Gaussian
Smear	350	10^{-6}	Methfessel-Paxton
All	400	10^{-8}	Methfessel-Paxton

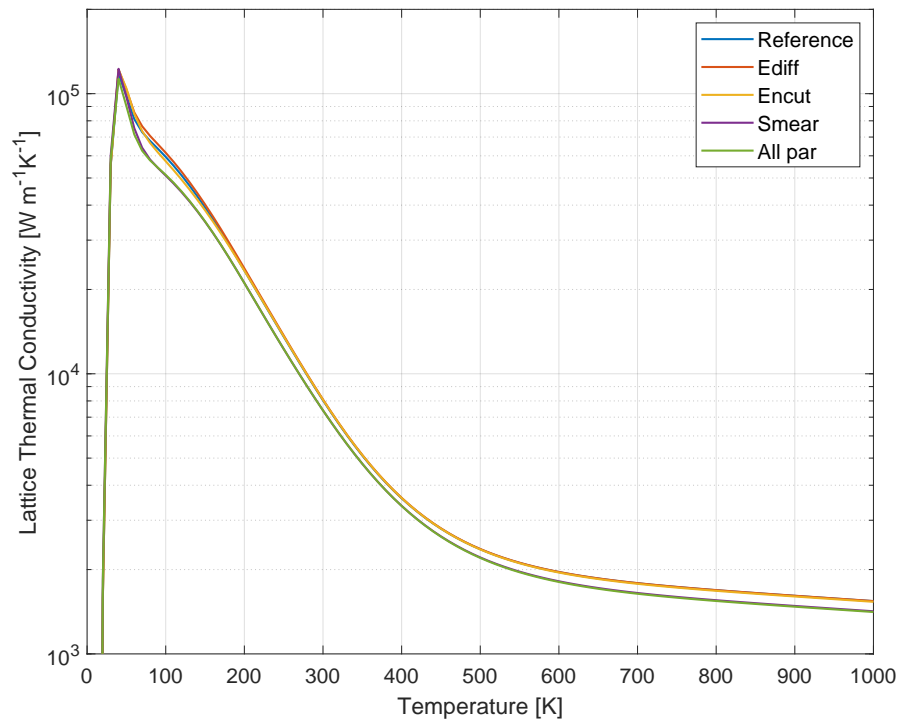


Figure 3.5: The effect of altering parameters in the force calculations.

This shows that no further improvement is made by increasing the parameters in table and justifies the usage of the reference settings.

Figure 3.6 shows the effects of executing the fc2 calculations on a larger supercell to reduce the numerical noise in the force calculations.

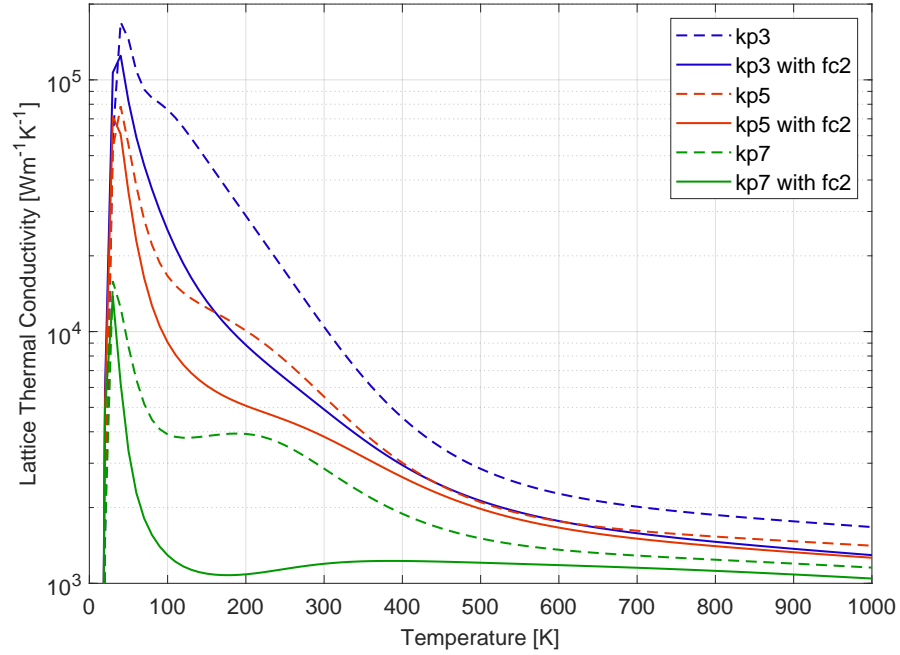


Figure 3.6: The effects of adding second order force calculations on a $2 \times 2 \times 2$ dimension supercell.

3.2 Effects of a vacancy

This section displays all results from the experiments conducted on the effects of a vacancy on the lattice thermal transport phenomena that is concerned in this thesis. The lattice thermal conductivity is investigated by evaluating the results in figure 3.7 where the LTC of the two models are plotted over a temperature interval. The phonon band structure is also modeled together with the total density of states for the phonons, and their results are displayed in figure 3.8 for the pristine supercell and in figure 3.9 for the supercell with one vacancy.

The two models referred to in this section are the pristine model corresponding to a perfect 16 atom supercell, and the vacancy model with 15 atoms where the center atom is replaced by a vacancy.

3.2.1 Lattice thermal conductivity

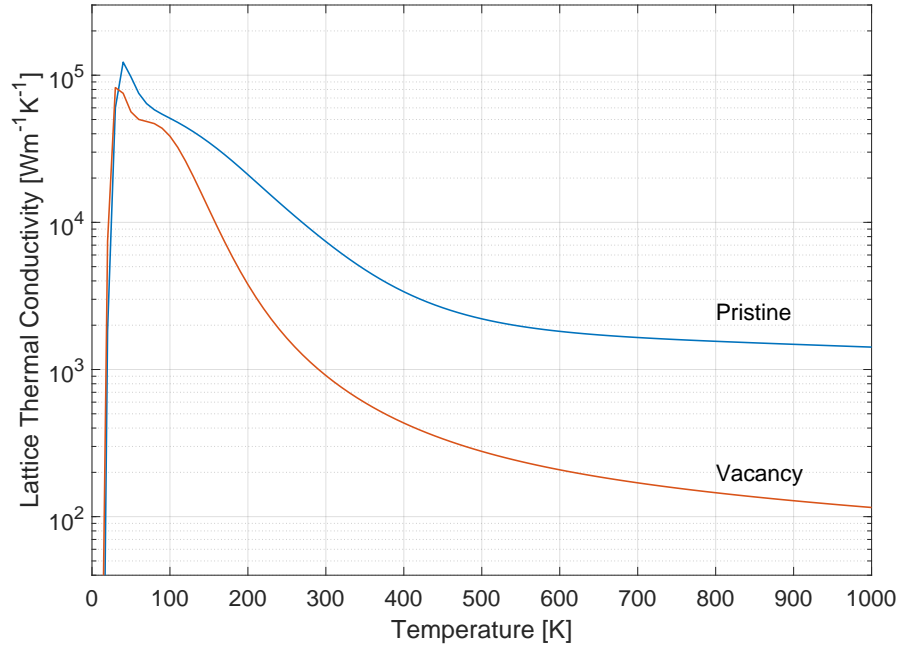


Figure 3.7: The LTC over a temperature range for the two models.

The curve marked pristine shows the LTC of a perfect 16 atom supercell, and the curve marked vacancy shows the LTC of a 15 atom supercell with one vacancy which yields a vacancy concentration of 6.25%.

3.2.2 Phonon band structure and density of states

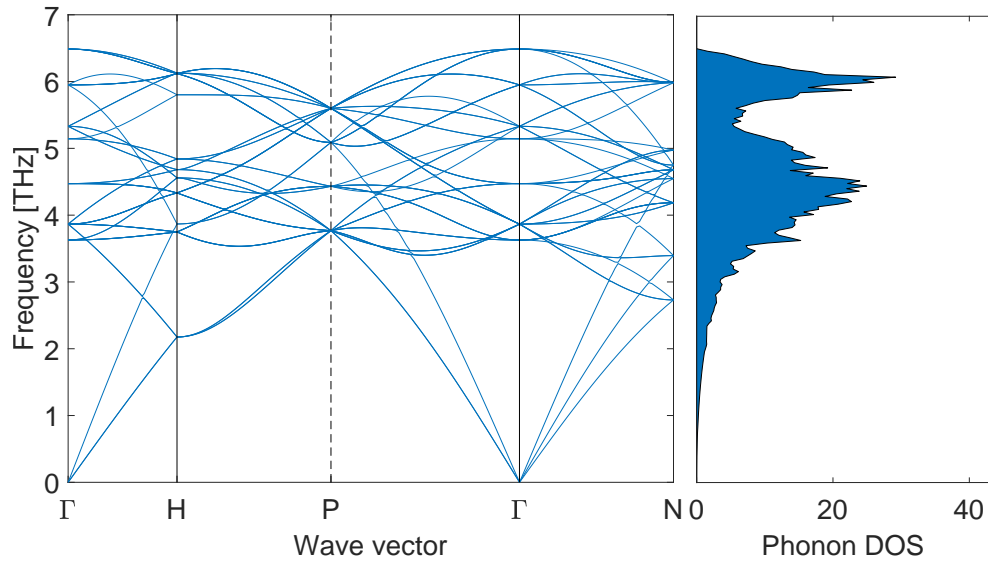


Figure 3.8: The phonon band structure together with the total density of states for the pristine model.

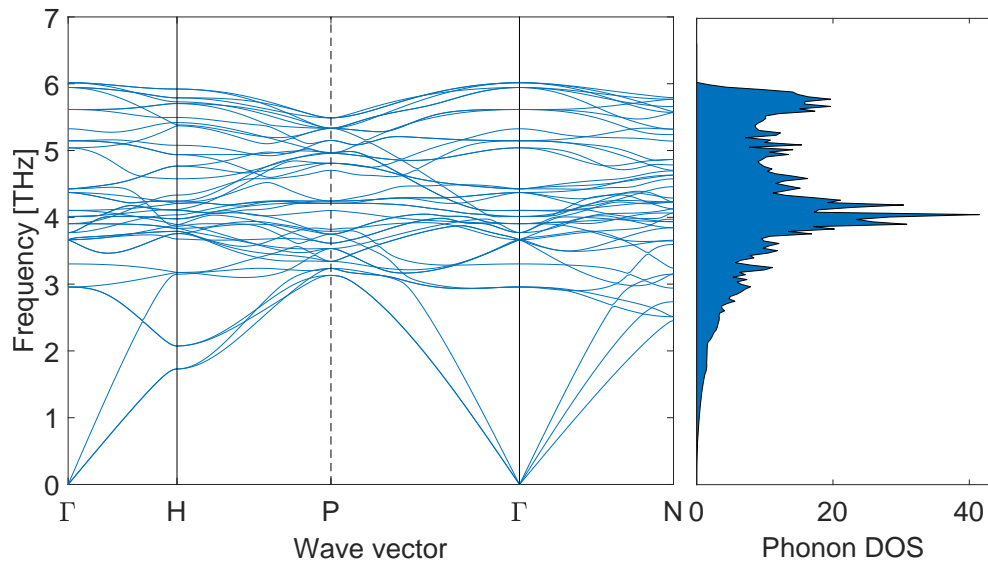


Figure 3.9: The phonon band structure together with the total density of states for the model containing a vacancy.

Chapter 4

Discussion

When reviewing the results of the convergence tests of the LTC in the last chapter, it is clear to see that the values are converged in itself, but far from converged towards the reference value and the only parameter that appears to have a positive effect is the addition of the second-order force constant calculations on a larger supercell. The discussion chapter will begin by evaluating these results.

The results of the experiment where the LTC is compared over an interval of k-points in figure 3.4 seem to converge to a higher value than expected. The reason for this is not known by the author and one theory is that the size of the supercells is too small in the models and this renders the boundary conditions set in the force calculators to be too narrow. This has not yet been thoroughly investigated, but there have been strong indications during the research that increasing the supercell size and therefore increasing the range of the plane-wave basis set would yield a more realistic value of the LTC.

The simulations where the fc2 is added show a positive effect on the LTC (figure 3.6) but unfortunately the computer performance limited further use of the setting. The standard setting in phono3py only calculates the obligatory fc3 which is sensitive to numerical noise in the force calculations, and by adding the fc2 calculations, the numerical noise is reduced. The fc2 is calculated by using the same settings as for the fc3 which makes it very time-consuming and the experiments on this are not thoroughly examined since the calculations are limited by computer performance. What is left to be tested, and believed by the author to give better results, is to reduce the number of k-points solely for the fc2 calculations. This should reduce both the requirements in performance

and amount of time. It is feasible since the fc2 calculations render a larger supercell than of the fc3 calculations. And by the fact that the reciprocal space is inversely proportional to real space, the reciprocal space of the larger supercell will be smaller than the original supercell and thus the number of k-points can be reduced for the fc2 calculations.

The central results of this work are the effects of a vacancy on the LTC which is displayed in figure 3.7. Although the accuracy of the LTC is unsatisfactory, the effects of a vacancy is still displaying the right trend which confirms the feasibility of the model. The LTC is roughly degraded by a factor of ten as a result of the vacancy and the magnitude of the degradation most likely depends on the vacancy concentration of the model. A vacancy concentration of $\frac{1}{16}$ is not realistic and no numerical conclusions should be taken from these results since the distortions yielded from a vacancy is interacting with its neighboring vacancies. But if the model were to be expanded to isolate the effects of one vacancy, the obtained values should be more trustworthy since the plane-wave basis set would return to its unperturbed nature in between the vacancy interactions.

The phonon band structure that is displayed in figure 3.8 and 3.9 together with the phonon density of states reveals that a vacancy affects the phonon frequency modes. The vacancy seems to have a splitting effect of the symmetry in the frequency bands since the simulation of the vacancy seems to contain a higher number of activated bands, and it has a canceling effect on the high frequency modes which degrades the heat capacity. And according to equation 1.21, the lattice thermal conductivity is dependent on the heat capacity. Besides the reduction of the mean-free path by the vacancy in the lattice, this could be an explanation to the degradation of the lattice thermal conductivity.

4.1 Social and ethical aspects

Nuclear power is considered being a reliable energy source with very low waste production and nearly complete absence of greenhouse gas emissions. These are two of the aspects that are of the highest focus when debating energy production and infrastructure expansion. On the other hand, a nuclear power plant is financially expensive and the energy production process comes with great risks that are in constant need to be managed.

The power generation process is a chain reaction of fission events where heavy

CHAPTER 4. DISCUSSION

atoms (e.g. ^{235}U) split and release heat which is transformed into electricity. Chain reactions are inherently unstable, but in nuclear power plants there are a number of passive safety systems. Still, the number of reactions per time unit needs to be controlled at all times. One of the greatest risks in operating a nuclear reactor is losing control of the heat management. If the cooling-process ceases to operate, the temperature in the reactor core would rise to extreme temperatures which could cause the core to melt.

Today, nuclear power-plants have emergency cooling-systems and are often contained in a concrete structure that protects the surrounding environment from the consequences of an accident. However, parts of the the public generally have an irrational fear for nuclear science arguably because it is easy to associate it with the accidents that have taken place or even nuclear weapons. This point of view is seemingly hard to change because it is emotionally anchored to the public ideologies and political affiliations.

In spite of the current reputation of nuclear power amongst the public, it is still believed by experts and specialists that nuclear technology is well worth being developed throughout the world to improve our society and infrastructure to make them more efficient, sustainable, and safer. This thesis is relevant to the safety and sustainability aspects of nuclear technology by providing knowledge on the irradiation effects and the thermal transport in metals.

Chapter 5

Conclusions and Future Work

5.1 Conclusions

The conclusions that can be drawn from this work is that this model shows that a vacancy has a substantial effect in degrading the lattice thermal conductivity but, to date, this model is not developed sufficiently enough to be able to draw any quantitative conclusions. The unrealistic vacancy concentration and the small supercell yielding too narrow boundary conditions are some reasons for the inaccuracy in the model.

One setting that gives a large positive effect in respect to computer cost is the setting that allows the second-order force constants to be calculated on a larger supercell. This is an option that should be subjected to a convergence test before utilizing further, but appears to have a very positive effect on the experiments performed in this work.

The effects of a vacancy on the lattice thermal conductivity is displaying the right trend which confirms that the model is feasible. A vacancy is also perturbing the nature of the phonons in the supercell by canceling some of the high-frequency modes. This suggests that phonons in the high-frequency modes are more effective in transporting heat which implies that the heat capacity increases with the phonon frequency.

The model is feasible, but more computer power and time is required to develop it further in order to make it numerically accurate.

5.2 Future work

For future work on this topic it is favorable to increase the supercell size in order to isolate the vacancy. In the current model of this work, the vacancy concentration is unrealistically large and the vacancies are interacting with its neighbors. If instead a larger supercell is built with 128 atoms, for instance, it is believed that the plane-wave basis would return to its undistorted nature in between vacancy interactions and thus the vacancy would be essentially isolated.

As seen in this report, the effects of the second-order force constants have a substantial effect on the LTC and it is highly suggested to use this setting in the future.

This model is also applicable to investigate the effects of a self-interstitial atom, namely the other part of the Frenkel-pair, which is also a product of the radiation damage process. And ultimately, if enough computer power and time is available, it is possible to investigate the effects of the whole thermal spike volume that is generated in the radiation damage process. What would also be interesting is to investigate the differences between BCC and FCC structures when it comes to degradation of the lattice thermal conductivity.

Hopefully this model can be expanded and used for research to aid the development of materials that better endures the radioactive environments in a nuclear power plant.

Chapter 6

Acknowledgement

In this text there is no doubt to whom I owe my deepest gratitude, namely to my supervisor professor Pär Olsson, head of Nuclear Engineering, department of physics at KTH. Thank you for supporting me through this work and assisting me in these dire times overshadowed by the Covid-19 pandemic. This period has undoubtedly been a challenge for us all and it is astonishing how you, overencumbered with work, still manages to aid me when needed.

Thank you my colleague Daniel for assisting me in the early stages of this work, your aid as been exceptionally important and it definitely helped to accelerate it further.

Thank you my dear Isabelle for not only showing blind and fathomless faith in me, but also rock-solid support. I am convinced that this is reflected in this work and I am sure that without you, this would not have been manageable.

And I would also like to thank my dear friends Viktor, Alexander, Jesse, and Tobias for snatching me away from work to enjoy your cheerful and delighted company. Upon returning to work I always felt rejuvenated and stronger than before. The same to my friends Daniel, Andreas, Henri, and Johan for your endless source of joy and support.

Last of all I would like to express my gratitude to my family, for always being there and doing everything in their power to aid me.

You all are very inspiring to me, and I hope that I can be an inspiration to you.

Chapter 7

References

- [1] W. Schilling, “Properties of frenkel defects,” *Journal of nuclear materials*, vol. 216, pp. 45–48, 1994.
- [2] M. Burton, “Radiation chemistry,” *The Journal of Physical Chemistry*, vol. 51, no. 2, pp. 611–625, 1947.
- [3] F. Seitz, “On the disordering of solids by action of fast massive particles,” *Discussions of the Faraday Society*, vol. 5, pp. 271–282, 1949.
- [4] A. Int, “1 e521-96 standard practice for neutron radiation damage simulation by charge-particle irradiation,” *Annual Book of ASTM Standards vol 12.02*.
- [5] K. Nordlund, S. J. Zinkle, A. E. Sand, F. Granberg, R. S. Averback, R. E. Stoller, T. Suzudo, L. Malerba, F. Banhart, W. J. Weber, *et al.*, “Primary radiation damage: A review of current understanding and models,” *Journal of Nuclear Materials*, vol. 512, pp. 450–479, 2018.
- [6] G. Kinchin and R. Pease, “The displacement of atoms in solids by radiation,” *Reports on progress in physics*, vol. 18, no. 1, p. 1, 1955.
- [7] M. Norgett, M. Robinson, and I. Torrens, “A proposed method of calculating displacement dose rates,” *Nuclear engineering and design*, vol. 33, no. 1, pp. 50–54, 1975.
- [8] L. Luneville, D. Simeone, and C. Jouanne, “Calculation of radiation damage induced by neutrons in compound materials,” *Journal of Nuclear Materials*, vol. 353, no. 1-2, pp. 89–100, 2006.

- [9] R. E. Stoller, M. B. Toloczko, G. S. Was, A. G. Certain, S. Dwaraknath, and F. A. Garner, “On the use of srim for computing radiation damage exposure,” *Nuclear instruments and methods in physics research section B: beam interactions with materials and atoms*, vol. 310, pp. 75–80, 2013.
- [10] J. Gigax, T. Chen, H. Kim, J. Wang, L. Price, E. Aydogan, S. A. Maloy, D. Schreiber, M. Toloczko, F. Garner, *et al.*, “Radiation response of alloy t91 at damage levels up to 1000 peak dpa,” *Journal of Nuclear Materials*, vol. 482, pp. 257–265, 2016.
- [11] K. Nordlund, A. E. Sand, F. Granberg, S. J. Zinkle, R. Stoller, R. S. Averback, T. Suzudo, L. Malerba, F. Banhart, W. J. Weber, *et al.*, “Primary radiation damage in materials. review of current understanding and proposed new standard displacement damage model to incorporate in cascade defect production efficiency and mixing effects,” tech. rep., Organisation for Economic Co-Operation and Development, 2015.
- [12] K. Nordlund, “Molecular dynamics simulation of ion ranges in the 1–100 keV energy range,” *Computational materials science*, vol. 3, no. 4, pp. 448–456, 1995.
- [13] T. D. De La Rubia, R. S. Averback, R. Benedek, and W. King, “Role of thermal spikes in energetic displacement cascades,” *Physical review letters*, vol. 59, no. 17, p. 1930, 1987.
- [14] M. T. Robinson, “Basic physics of radiation damage production,” *Journal of nuclear materials*, vol. 216, pp. 1–28, 1994.
- [15] G. S. Was, *Fundamentals of radiation materials science: metals and alloys*. springer, 2016.
- [16] Y. A. Nikolaev, A. Nikolaeva, and Y. I. Shtrombakh, “Radiation embrittlement of low-alloy steels,” *International journal of pressure vessels and piping*, vol. 79, no. 8-10, pp. 619–636, 2002.
- [17] B. Gurovich, E. Kuleshova, Y. A. Nikolaev, and Y. I. Shtrombakh, “Assessment of relative contributions from different mechanisms to radiation embrittlement of reactor pressure vessel steels,” *Journal of Nuclear Materials*, vol. 246, no. 2-3, pp. 91–120, 1997.
- [18] M. Li and S. Zinkle, “Deformation mechanism maps of unirradiated and irradiated v-4cr-4ti,” *Journal of ASTM International*, vol. 2, no. 10, pp. 1–17, 2005.

CHAPTER 7. REFERENCES

- [19] J. Matthews and M. Finnis, “Irradiation creep models—an overview,” *Journal of Nuclear Materials*, vol. 159, pp. 257–285, 1988.
- [20] V. Fidleris, “The irradiation creep and growth phenomena,” *Journal of Nuclear Materials*, vol. 159, pp. 22–42, 1988.
- [21] J. Foster, W. Wolfer, A. Biancheria, and A. Boltax, “Analysis of irradiation-induced creep of stainless steel in fast spectrum reactors,” tech. rep., Westinghouse Electric Corp., Madison, Pa.(USA). Advanced Reactors Div., 1972.
- [22] S. J. Zinkle, H. Tanigawa, and B. D. Wirth, “Radiation and thermomechanical degradation effects in reactor structural alloys,” in *Structural Alloys for Nuclear Energy Applications*, pp. 163–210, Elsevier, 2019.
- [23] E. Gilbert and J. Bates, “Dependence of irradiation creep on temperature and atom displacements in 20% cold worked type 316 stainless steel,” in *Measurement of Irradiation-enhanced Creep in Nuclear Materials*, pp. 204–209, Elsevier, 1977.
- [24] W. Jones and N. H. March, *Theoretical solid state physics*, vol. 35. Courier Corporation, 1985.
- [25] S. Stackhouse and L. Stixrude, “Theoretical methods for calculating the lattice thermal conductivity of minerals,” *Reviews in Mineralogy and Geochemistry*, vol. 71, no. 1, pp. 253–269, 2010.
- [26] L. Snead, S. Zinkle, and D. White, “Thermal conductivity degradation of ceramic materials due to low temperature, low dose neutron irradiation,” *Journal of nuclear materials*, vol. 340, no. 2-3, pp. 187–202, 2005.
- [27] L. Boltzmann, “Weitere studien über das wärmegleichgewicht unter gasmolekülen,” in *Kinetische Theorie II*, pp. 115–225, Springer, 1970.
- [28] G. Srivastava, *The Physics of Phonons*. CRC Press, 1990.
- [29] P. T. Alvarez, *Thermal transport in semiconductors: first principles and phonon hydrodynamics*. Springer, 2018.
- [30] A. C. Sparavigna, “The boltzmann equation of phonon thermal transport solved in the relaxation time approximation–i–theory,” 2016.
- [31] J. Callaway, “Model for lattice thermal conductivity at low temperatures,” *Physical Review*, vol. 113, no. 4, p. 1046, 1959.

- [32] M. Born and R. Oppenheimer, “Zur quantentheorie der molekeln,” *Annalen der physik*, vol. 389, no. 20, pp. 457–484, 1927.
- [33] P. Hohenberg and W. Kohn, “Inhomogeneous electron gas,” *Physical review*, vol. 136, no. 3B, p. B864, 1964.
- [34] W. Kohn and L. J. Sham, “Self-consistent equations including exchange and correlation effects,” *Physical review*, vol. 140, no. 4A, p. A1133, 1965.
- [35] N. Harrison, “An introduction to density functional theory,” *Nato Science Series Sub Series III Computer and Systems Sciences*, vol. 187, pp. 45–70, 2003.
- [36] L. H. Thomas, “The calculation of atomic fields,” in *Mathematical Proceedings of the Cambridge Philosophical Society*, vol. 23, pp. 542–548, Cambridge University Press, 1927.
- [37] D. Ceperley and B. Alder, “Exchange-correlation potential and energy for density-functional calculation,” *Phys. Rev. Lett*, vol. 45, pp. 567–581, 1980.
- [38] V. Karasiev, T. Sjostrom, J. Dufty, and S. Trickey, “Local density approximation exchange-correlation free-energy functional,” in *APS March Meeting Abstracts*, 2014.
- [39] M. Nekovee, W. Foulkes, and R. Needs, “Quantum monte carlo analysis of exchange and correlation in the strongly inhomogeneous electron gas,” *Physical review letters*, vol. 87, no. 3, p. 036401, 2001.
- [40] G. Kresse and J. Hafner, “Ab initio molecular dynamics for liquid metals,” *Physical Review B*, vol. 47, no. 1, p. 558, 1993.
- [41] G. Kresse and J. Furthmüller, “Vasp the guide (universität wien, wien, austria, 2007),” *Phys. Rev. B*, vol. 47, p. 558, 1993.
- [42] P. E. Blöchl, “Projector augmented-wave method,” *Physical review B*, vol. 50, no. 24, p. 17953, 1994.
- [43] A. Togo, L. Chaput, and I. Tanaka, “Distributions of phonon lifetimes in brillouin zones,” *Physical Review B*, vol. 91, no. 9, p. 094306, 2015.
- [44] A. Togo and I. Tanaka, “First principles phonon calculations in materials science,” *Scripta Materialia*, vol. 108, pp. 1–5, 2015.

CHAPTER 7. REFERENCES

- [45] I. Mathematica's ElementData function from Wolfram Research, "Lattice constants of the elements," <https://periodictable.com/Properties/A/LatticeConstants.html>, visited 2020-04-28.
- [46] B. Medasani, M. Haranczyk, A. Canning, and M. Asta, "Vacancy formation energies in metals: A comparison of metagga with lda and gga exchange–correlation functionals," *Computational Materials Science*, vol. 101, pp. 96–107, 2015.
- [47] Y. Kraftmakher, "Equilibrium vacancies and thermophysical properties of metals," *Physics Reports*, vol. 299, no. 2-3, pp. 79–188, 1998.
- [48] S. Kanpara, S. Khirwadkar, S. Belsare, K. Bhope, R. Swamy, Y. Patil, P. Mokariya, N. Patel, T. Patel, and K. Galodiya, "Fabrication of tungsten & tungsten alloy and its high heat load testing for fusion applications," *Materials Today: Proceedings*, vol. 3, no. 9, pp. 3055–3063, 2016.

TRITA ITM-EX 2020:308